Author/s:
Thalassinos, G;McCloskey, DJ;Mameli, A;Healey, AJ;Pattinson, C;Simpson, D;Gibson, BC;Stacey, A;Dontschuk, N;Reineck, P

Title:
Robust quantification of the diamond nitrogen-vacancy center charge state via photoluminescence spectroscopy

Date:
2025-10-01

Citation:
Thalassinos, G., McCloskey, D. J., Mameli, A., Healey, A. J., Pattinson, C., Simpson, D., Gibson, B. C., Stacey, A., Dontschuk, N. & Reineck, P. (2025). Robust quantification of the diamond nitrogen-vacancy center charge state via photoluminescence spectroscopy. APL Photonics, 10 (10), pp.101102-. https://doi.org/10.1063/5.0284237.

Persistent Link:
https://hdl.handle.net/11343/369279

TUTORIAL | OCTOBER 22 2025

Robust quantification of the diamond nitrogen-vacancy center charge state via photoluminescence spectroscopy

G. Thalassinos ; D. J. McCloskey ; A. Mameli ; A. J. Healey ; C. Pattinson ; D. Simpson ; B. C. Gibson ; A. Stacey ; N. Dontschuk ; P. Reineck

APL Photonics 10, 101102 (2025)
https://doi.org/10.1063/5.0284237

Robust quantification of the diamond nitrogen-vacancy center charge state via photoluminescence spectroscopy

Cite as: APL Photon. 10, 101102 (2025); doi: 10.1063/5.0284237
Submitted: 6 June 2025 • Accepted: 2 October 2025 •
Published Online: 22 October 2025

G. Thalassinos,[1,a] D. J. McCloskey,[2,3] A. Mameli,[1] A. J. Healey,[1] C. Pattinson,[2,3] D. Simpson,[2,3] B. C. Gibson,[1] A. Stacey,[1,4] N. Dontschuk,[2,b] and P. Reineck[1,c]

AFFILIATIONS

[1] School of Science, RMIT University, Melbourne, VIC 3001, Australia
[2] School of Physics, University of Melbourne, Parkville, VIC 3010, Australia
[3] Australian Research Council Centre of Excellence in Quantum Biotechnology, School of Physics, University of Melbourne, Parkville, VIC 3010, Australia
[4] Princeton Plasma Physics Laboratory, Princeton University, Princeton, New Jersey 08540, USA

[a] **Author to whom correspondence should be addressed:** giannis.thalassinos@rmit.edu.au
[b] **Electronic mail:** dontschuk.n@unimelb.edu.au
[c] **Electronic mail:** philipp.reineck@rmit.edu.au

ABSTRACT

Nitrogen vacancy (NV) centers in diamond are at the heart of many emerging quantum technologies, all of which require control over the NV charge state. Hence, methods for quantification of the relative photoluminescence intensities of the NV^0 and NV^- charge states, i.e., a charge state ratio, are vital. Several approaches to quantify NV charge state ratios have been reported but are either limited to bulk-like NV diamond samples or yield qualitative results. We propose an NV charge state quantification protocol based on the determination of sample- and experimental setup-specific NV^0 and NV^- reference spectra. The approach employs blue (400–470 nm) and green (480–570 nm) excitation to infer pure NV^0 and NV^- spectra, which are then used to quantify NV charge state ratios in subsequent experiments via least squares fitting. We test our dual excitation protocol (DEP) for a bulk diamond NV sample and 20 and 100 nm nanodiamond particles and compare results with those obtained via other commonly used techniques such as zero-phonon line fitting and non-negative matrix factorization. We find that DEP can be employed across different samples and experimental setups and yields consistent and quantitative results for NV charge state ratios that are in agreement with our understanding of NV photophysics. By providing robust NV charge state quantification across sample types and measurement platforms, DEP will support the development of NV-based quantum technologies.

I. INTRODUCTION

The nitrogen vacancy (NV) center in diamond is one of the most widely adopted platforms for emerging quantum technologies.[1–3] In bulk diamond, NV centers are generally present in either a neutral (NV^0) or a negative charge state (NV^-). Although both charge states are photoluminescent, only NV^- has an optically addressable spin that allows for spin-based optical quantum sensing, enabling applications including magnetometry[4] and thermometry.[5] Furthermore, the NV charge state itself can be used as an all-optical nanoscale voltage[6] and electric-field sensor.[7] Hence, significant materials engineering[8] and photonics[9,10] efforts are underway to control and tailor the NV charge state for specific applications.

Underpinning all of these efforts is the ability to quantify the NV charge state. While the two charge states can be clearly identified in photoluminescence (PL) spectra via their zero-phonon lines (ZPLs) at 575.07 nm (2.156 eV, NV^0) and 637.45 nm (1.945 eV, NV^-), their phonon sidebands (PSBs) overlap significantly [Fig. 1(a)],[11–13] making precise quantification of the relative contribution of each charge state to the overall NV PL non-trivial. Several approaches for the quantification of the NV charge state

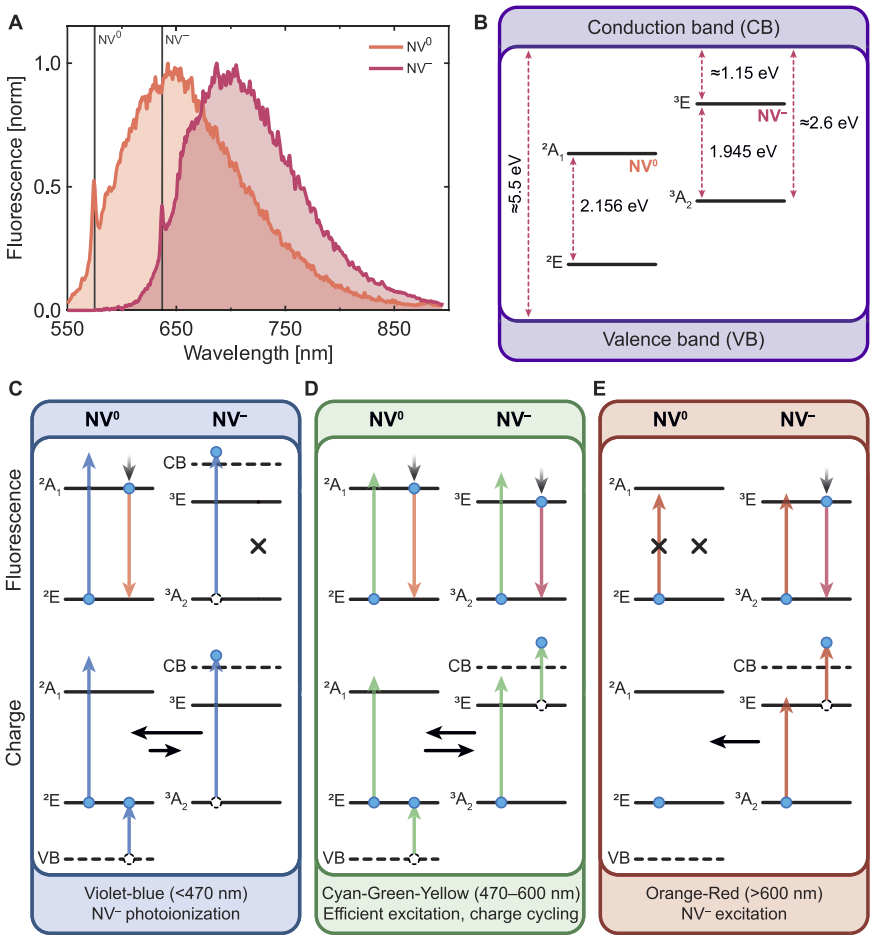

FIG. 1. NV center photodynamics. (a) Fluorescence spectra of NV^0 and NV^- with characteristic ZPLs at 575 and 637 nm (marked via vertical lines), respectively, showing significant overlap between 600 and 850 nm. (b) Energy level diagram of NV^0 and NV^- within the diamond bandgap. (c)–(e) Dynamics of the NV center under different excitation wavelengths. Violet-blue excitation (c) leads to single-photon photoionization of NV^- into NV^0, while still exciting NV^0, which relaxes down to the ground state via fluorescence. Green illumination (d) leads to efficient excitation of both charge states and allows for dynamic charge state switching via ionization and re-pumping processes. Red light (e) has insufficient energy to promote NV^0 to the excited state, leading exclusively to NV^- emission. Horizontal black lines indicate charge state switching, with relative lengths indicative of the rate in a particular direction. Vertical short gray lines represent phonon relaxations.

have been reported. One approach uses the intensity ratio of the two ZPLs as a measure of the relative contribution of each charge state to the overall PL signal.[14–17] This approach is feasible for NV ensemble measurements in bulk diamond samples, where pronounced NV ZPLs are generally observed, particularly at low temperatures.[18] However, for NV centers in small nanodiamonds[11,19,20] and, more generally, for NV centers within a few nanometers of the diamond surface,[6] ZPLs are weak or not visible at all in PL spectra. Therefore, another approach to quantify the NV charge state ratio is based on the use of "pure" NV^0 and NV^- spectra from the literature, such as Ref. 11, that are used as fits in other laboratories.[21–23] However, NV spectral profiles can vary depending on the diamond properties (e.g., strain), sample dimensions (bulk vs nanoparticles), environmental factors like temperature,[24,25] the nanoscale environment,[26] and the spectroscopy equipment used. As a result, the seemingly simple question, "How far into the far-red do NV^0 and NV^- emit?" has no simple answer based on the current literature (see the supplementary material, Table S1). Hence, pure NV^0 and NV^- spectra are ideally acquired in a sample- and equipment-specific manner.

To this end, three main approaches have been reported. The first two approaches are photoluminescence (PL) decomposition analysis[15] and a similar microwave-assisted decomposition technique.[25] The former modulates the NV charge state via the excitation power to change the NV^- ionization rate; the latter modulates the NV^- PL intensity using microwaves. Both techniques use their respective modulation to first derive the spectral profile of NV^-. Then, this NV^- reference is subtracted from a mixed NV^0/NV^- signal until there is no visible ZPL peak at 637 nm to determine NV^0. The third approach employs machine learning, which does not require *a priori* knowledge about the NV ZPLs in order to derive a set of pure NV spectra. Non-negative matrix factorization (NNMF) is an often-used algorithm for the decomposition of spectra into an integer number of non-negative components for a given set of training data. The training set consists of a series of NV spectra, where each spectrum contains different relative contributions of NV^0 and NV^-.[27–30] However, it is not clear that NNMF accurately determines the "true" NV^0/NV^- spectral profiles. Compared to experiments,[11–13,15,18,22,25,31–33] NNMF predicts that the maximum emission wavelength of NV^0 is significantly shorter than NV^- by >70 nm (see the supplementary material, Table S1)[27–30] and can show the presence of the NV^- ZPL in the "pure" NV^0 spectrum and/or vice versa.[29] Therefore, new approaches are needed.

Here, we propose a dual wavelength excitation protocol (DEP) for measuring the pure NV^0 and NV^- spectral profiles, which are

used to determine the NV charge state ratio. We show that this method works across a wide variety of diamond types, including bulk diamond and nanoparticles, and vastly different optical configurations, including confocal microscopes and nanoparticles in suspension. We leverage the direct photoionization of NV^- using blue/violet excitation (<470 nm) to obtain a pure NV^0 spectrum, which is then used to determine the NV^- spectrum. NV^0 and NV^- reference spectra are then fit to experimental data using the linear least-squares fitting algorithm to determine the NV charge state ratio. We benchmark this technique against ZPL fitting, NNMF, and skewed Gaussian (SG) fitting to approximate the "pure" NV spectra. We demonstrate that our protocol works across a range of samples and measurement techniques, even in the absence of ZPLs. Our protocol enables robust quantification of the NV charge state and will thereby aid the development of next-generation quantum sensing materials and protocols.

II. METHODS

A. Confocal fluorescence spectroscopy

We investigated a commercially available bulk diamond sample (DNV-B14, Element Six) and fluorescent nanodiamonds (FNDs) with a nominal diameter of 100 nm (Adàmas Nanotechnologies) spin-coated onto a Si substrate using our custom-built scanning confocal microscope (see the supplementary material, Fig. S1A). Samples were excited using an 80 MHz pulsed laser (Fianium WhiteLase 400-SC, NKT Photonics) operating between 400 and 700 nm through a 100× objective (NA = 0.9). Fluorescence was collected through the same objective and fiber coupled to an avalanche photodiode (APD) (25%, SPCM-AQRH-14-TR, Excelitas) and a spectrometer (75%, SpectraPro SP-2500, Princeton Instruments) with a charge-coupled device (CCD) camera (PIXIS 100BR, Princeton Instruments).

B. In-solution fluorescence spectroscopy

Fluorescent nanodiamonds (FNDs) with nominal sizes of 20 and 140 nm (Adámas Nanotechnologies) were suspended in deionized (DI) water at ~1.00 and 0.01 mg ml^{-1}, respectively, before being measured in our custom-built in-solution spectroscopy setup (see the supplementary material, Fig. S1B). Samples were excited using the same pulsed laser as the confocal setup and weakly focused onto the sample cuvette (18FL, FireFlySci). Fluorescence was collected via a custom fiber (105 μm core, NA = 0.22) through an in-line filter mount (FOFMS, Thorlabs) and coupled into the spectrometer. For each excitation wavelength, a water Raman spectrum and a scattering reference using 40 nm SiO_2 nanoparticles were acquired and subtracted from the FND signals (see the supplementary material for details).

III. DUAL EXCITATION PROTOCOL

Generally, accurately determining the spectral profile of NV^- can be achieved using any technique that requires at least two measured spectra with a different NV charge state ratio.[15,25,27,28,30] The fundamental challenge lies in the robust determination of the NV^0 spectral profile in the spectral region above 700 nm, where it significantly overlaps with NV^-.

While the NV^- ^3E excited state is ≈1.15 eV below the conduction band (CB),[34,35] the $^3A_2$ ground state can be photoionized to the NV^0 ^2E ground state via a single-photon process using photon energies of ≈2.6–2.7 eV (or ≈470 nm).[13,36] In practice, it has been observed that NV PL spectra acquired using excitation wavelengths of 458 nm[12,37] still show some NV^- PL in bulk diamond, which disappears for excitation wavelengths <450 nm. Under green excitation (510–540 nm), both NV charge states are efficiently excited and cycle between each other through ionization and recombination processes [Fig. 1(d)].[13] Under red excitation (600–640 nm), photons only have sufficient energy to excite NV^- [Fig. 1(e)]. Simply, there exist excitation windows in which either one of the two NV charge states is directly excited, or both are. Therefore, by tuning the excitation wavelength, sample-specific reference NV^0/NV^- spectra can be obtained.

Figure 2 illustrates the main steps of our protocol based on measurements performed on commercially available fluorescent

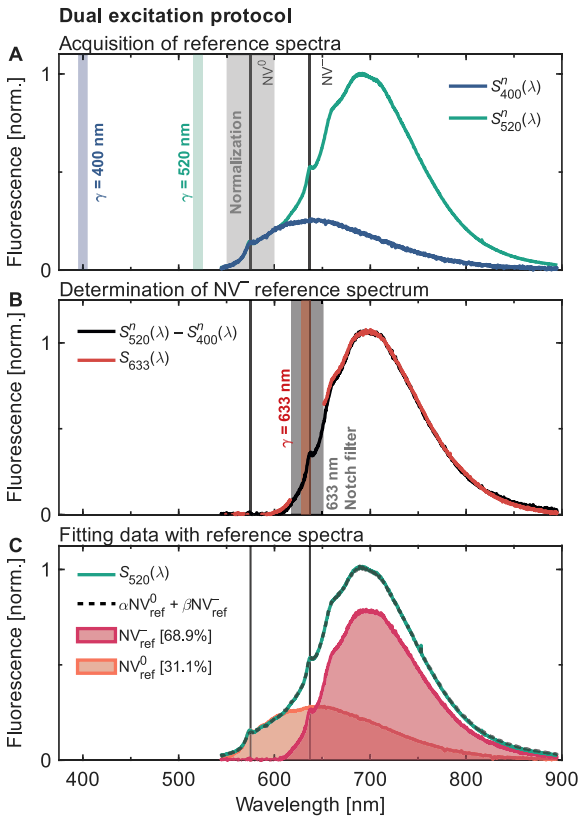

FIG. 2. Dual excitation protocol on 140 nm FNDs suspended in water. (a) Reference spectra are acquired using 400 and 520 nm excitation to obtain a pure NV^0 signal $[S^n_{400}(\lambda)]$ and a mixed NV^0/NV^- spectrum $[S^n_{520}(\lambda)]$, respectively, which are then normalized for the same NV^0 contribution between 550 and 600 nm (shaded region). (b) A pure NV^- spectrum is obtained by taking the difference between the two reference spectra in (a), which is then compared to the experiment under 633 nm illumination $[S_{633}(\lambda)]$. (c) The reference NV^0 and NV^- spectra can then be used to fit experimental data using Eq. (1) to determine the charge state ratio.

nanodiamonds (FNDs) with a nominal size of 140 nm suspended in DI water. Pure NV^0 and mixed NV^0/NV^- fluorescence spectra were acquired using violet (400 nm) and green (520 nm) excitation, respectively, as shown in Fig. 2(a). The measured spectra are labeled $S_\gamma(\lambda)$, where γ and λ represent the excitation and emission wavelengths, respectively.

Each measured NV signal can be expressed as a linear combination of the two charge states

$$S_\gamma(\lambda) = \alpha(\gamma)\mathrm{NV}^0 + \beta(\gamma)\mathrm{NV}^-, \tag{1}$$

where $\alpha(\gamma)$ and $\beta(\gamma)$ are unknown non-negative scalar quantities representing the relative contribution of each charge state as a function of the excitation wavelength. In the case where $\gamma < 470$ nm, $\alpha > 0$, and we assume $\beta \approx 0$, yielding us a reference NV^0 spectrum (NV^0_{ref}),

$$S_{<470}(\lambda) = \alpha(<470)\mathrm{NV}^0 = \mathrm{NV}^0_{\mathrm{ref}}. \tag{2}$$

NV^- exhibits negligible fluorescence below 600 nm;[12] therefore, both spectra were normalized (denoted by superscript n) between λ_i = 550–600 nm [highlighted in gray in Fig. 2(a)], via the expression

$$S^n_\gamma(\lambda) = \frac{S_\gamma(\lambda)}{\sum_i S_\gamma(\lambda_i)}. \tag{3}$$

Therefore, both spectra are normalized such that the area under the curve between 550 and 600 nm is equal to 1; therefore, both spectra are normalized to the same NV^0 intensity, or

$$\frac{\alpha(<470)}{\alpha(520)} = 1. \tag{4}$$

This normalization allows us to fully subtract the NV^0 signal from any mixed NV^0/NV^- spectrum, resulting in a pure NV^- reference spectrum (NV^-_{ref}), via the relation

$$\mathrm{NV}^-_{\mathrm{ref}} = S^n_{470-600}(\lambda) - S^n_{<470}(\lambda), \tag{5}$$

as seen in Fig. 2(b). Here, we see that the NV^- ZPL correctly appears at 637 nm, with no sign of NV^0 fluorescence. For verification, we investigated the same sample under 633 nm (1.959 eV) excitation, which only has sufficient energy to excite NV^-, labeled $[S_{633}(\lambda)]$. We found that red excitation leads to no detectable NV^0 signal and is nearly identical to the DEP derived NV^- spectrum.

With these two measurements, we can fit any combination of NV^0 and NV^- using the least squares method to precisely determine the NV charge state ratio, which we quantify here as the NV^- contribution divided by the total NV (NV_T) fluorescence originating from the diamond, via the expression

$$\frac{\mathrm{NV}^-}{\mathrm{NV_T}} = \frac{\beta(\gamma)\int_{\lambda=0}^{\inf}\mathrm{NV}^-_{\mathrm{ref}}(\lambda)\,d\lambda}{\int_{\lambda=0}^{\inf}\alpha(\gamma)\mathrm{NV}^0_{\mathrm{ref}}(\lambda) + \beta(\gamma)\mathrm{NV}^-_{\mathrm{ref}}(\lambda)\,d\lambda}. \tag{6}$$

An example is provided in Fig. 2(c), where the two reference spectra are used to fit the original green data $[S_{520}(\lambda)]$, revealing an NV^- contribution of 68.9%.

A. Benchmarking

We tested our protocol for three different samples across two measurement techniques. First, we investigated a commercially available bulk diamond sample with clear NV ZPLs under a confocal microscope, representing the simple case. Second, we suspended an ensemble of 20 nm FNDs in DI water and analyzed them using our in-solution setup. Finally, we analyzed 100 nm FND particles under a confocal microscope. For each test case, we compared our protocol against three other methods for determining the charge state ratio: ZPL fitting, fitting a skewed Gaussian (SG) model, and NNMF (see the supplementary material for details).

We excited the bulk sample using a tunable laser from 405 to 520 nm (bandwidth of 10 nm) at a constant power of 5 μW using a custom-built confocal microscope. Normalized fluorescence spectra acquired using different excitation wavelengths are shown in Fig. 3(a). The spectra show mostly NV^0 PL for excitation wavelengths 405–470 nm. For longer wavelengths, the NV^- contribution continuously increases up to the highest investigated excitation wavelength of 520 nm. The spectra were then analyzed using the different methods mentioned earlier to determine the NV^- ratio as a function of excitation wavelength [Fig. 3(b); for fitting of individual spectra using each technique, see the supplementary material, Figs. S2–S5]. All protocols yield a constant NV ratio below 470 nm excitation, which then increases with excitation wavelength up to 520 nm excitation. DEP, NNMF, and SG fitting were all capable of fitting each combination of NV^0 and NV^- with an R^2 of >0.98, with NNMF being the highest on average (see the supplementary material, Fig. S6). Both DEP and ZPL fittings yield an NV^- ratio of 0% below 470 nm excitation, which increases to 60% as the excitation wavelength increases to 520 nm. SG and NNMF, on the other hand, yield a significantly higher minimum NV^- contribution of 10% and 40%, respectively, below 470 nm excitation, which increases to 70% and 80% for 520 nm excitation.

Assuming that excitation below 450 nm should result in pure NV^0 fluorescence,[12,13,38] the presence of NV^- in these fits is indicative of an underestimate of how far into the red spectral region the NV^0 emission extends. Indeed, the NNMF output for the pure NV^0 spectrum (see the supplementary material, Fig. S7) suggests that NV^0 does not emit above 750 nm, while our measurements using 400 nm excitation suggest that NV^0 emission extends well above 800 nm. Overall, the data in Figs. 3(a) and 3(b) show that both DEP and ZPL fitting yield very similar results in this case, both of which are in agreement with our current understanding of NV charge state photophysics. Both NNMF and SG methods, even in this relatively simple case, overestimate the NV^- contribution to the NV PL spectra.

As a second, more challenging test case, we investigated an ensemble of commercially available 20 nm FNDs suspended in water. FNDs of this size typically show predominantly NV^0 PL, and the ZPLs of both charge states are weak and, in some cases, not visible at all.[19,28] Figure 3(c) shows normalized PL spectra of the 20 nm FNDs in suspension as a function of 520 nm laser excitation power in the range from 0.6 to 22 mW. The PL spectra slightly redshift with increasing excitation power, which suggests an increase in the NV^- contribution with increasing excitation power caused by increased photocycling rates.

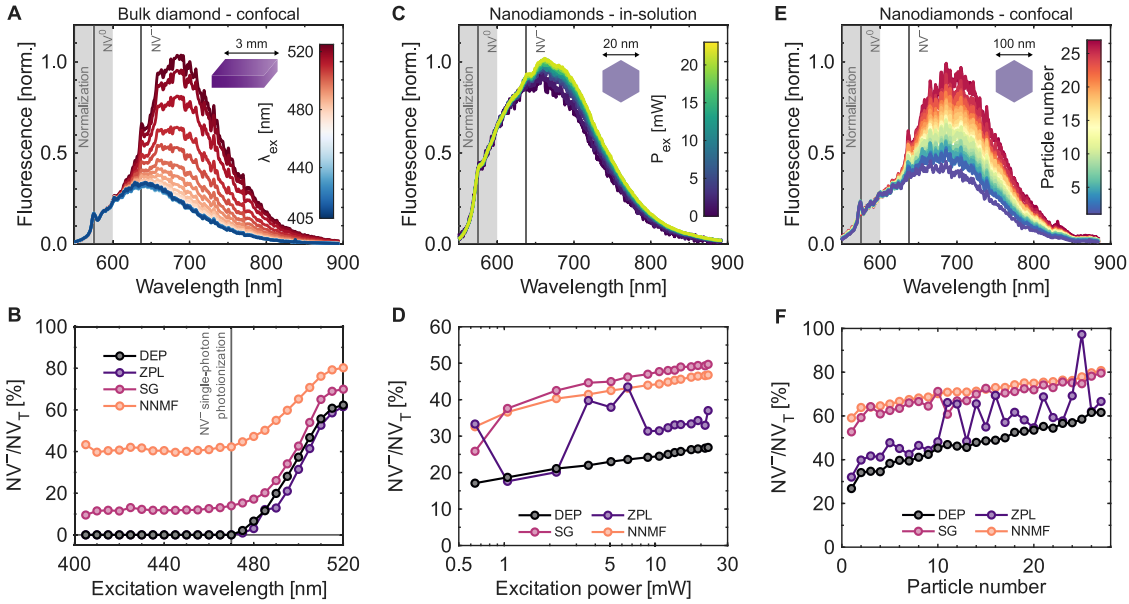

FIG. 3. NV charge state ratio protocol comparison quantified as the NV^- contribution defined in Eq. (6). (a) Fluorescence spectra of bulk diamond for excitation wavelengths (λ_{ex}) ranging from 405 to 520 nm under a confocal microscope. (b) NV^- contribution of the bulk diamond using our dual-excitation protocol (DEP), ZPL, Skewed Gaussian (SG), and NNMF fitting. The vertical line roughly indicates the wavelength we expect to see single-photon photoionization of NV^-. (c) Fluorescence spectra of 20 nm FNDs suspended in DI water, excited using 520 nm for excitation powers (P_{ex}) between 0.64 and 22.30 mW. (d) NV^- contribution of the 20 nm FNDs as a function of excitation power. (e) Fluorescence spectra of dispersed 100 nm FNDs under a confocal microscope, ordered by increasing NV^- content. (f) NV^- contribution for all 100 nm particles using each protocol. All spectra [(a), (c), and (e)] were normalized between 550 and 600 nm (shaded regions), with vertical lines marking the positions of the NV ZPLs.

We again used the four different analysis approaches to quantify the above-mentioned observations, with results shown in Fig. 3(d). DEP yields a monotonic increase in the NV^- ratio from 17% to 27% with increasing excitation power. While SG and NNMF yield a comparable relative increase in the NV^- contribution with increasing excitation power, both appear to overestimate the absolute NV^- ratio by up to 24%. ZPL fitting yields inconsistent results, though these are typically bounded by the values obtained from the other analysis techniques. ZPL fitting is inconsistent mainly because peak fitting becomes extremely sensitive to minor changes in both signal and noise for weak ZPLs, such as those observed in 20 nm FNDs. Given the relative importance of near-surface NV centers in bulk diamond and FNDs in current research, the ability of DEP to quantify small changes in the NV^- ratio even in the absence of strong ZPLs is a major strength of our technique.

Finally, we tested our approach for 100 nm FNDs dispersed on a silicon wafer substrate, imaged with a scanning confocal fluorescence microscope connected to a spectrometer. We collected PL spectra for 27 FNDs (or small FND aggregates) using 405 and 520 nm excitation (the fluorescence map with marked FNDs can be found in the supplementary material, Fig. S8). We averaged all spectra acquired using 405 nm excitation to be used as the NV^0 reference for DEP. The PL spectrum for each particle was normalized and ordered by increasing NV^- PL intensity, quantified as the integrated fluorescence above 650 nm divided by the integrated fluorescence below 650 nm, as shown in Fig. 3(e). Here, we see significant variability in the NV charge state ratio between individual particles, with some consisting almost entirely of NV^0 while others show predominantly NV^-, consistent with prior reports.[27] Figure 3(f) shows the NV^- ratio determined by all four analysis approaches for all particles. As observed in the previous two test cases, both SG and NNMF yield a higher NV^- contribution, ranging from ≈55% to 80%, compared to both ZPL and DEP [Fig. 3(f)]. DEP suggests the NV^- contribution ranges from 27% to 62% with an average of 47% ± 9%. For many particles, ZPL fitting and DEP yield very similar results. However, since the ZPL lines are very pronounced for some particles and are barely visible for others, the NV^- ratios determined using the ZPL fitting approach are quite susceptible to artifacts and, consequently, exhibit far greater variation. We do not, therefore, attribute the observed variation to intrinsic properties of the analyzed particles.

B. Workflow

We propose a simple workflow for the implementation of our protocol, which is summarized in Fig. 4. Only two primary measurements (Fig. 4, top row) are required for the determination of pure NV^- and NV^0 reference spectra: one PL spectrum acquired using green (480–570 nm) excitation that contains contributions from both charge states and one PL spectrum acquired using blue (<470 nm) excitation for a pure NV^0 spectrum. Next, all background signals must be acquired and removed from the two reference spectra. Background signals are system and sample dependent, but in many cases, this step may only require a simple background subtraction due to detector dark counts. In some cases, however, background signals may be more complex, such as Raman signals

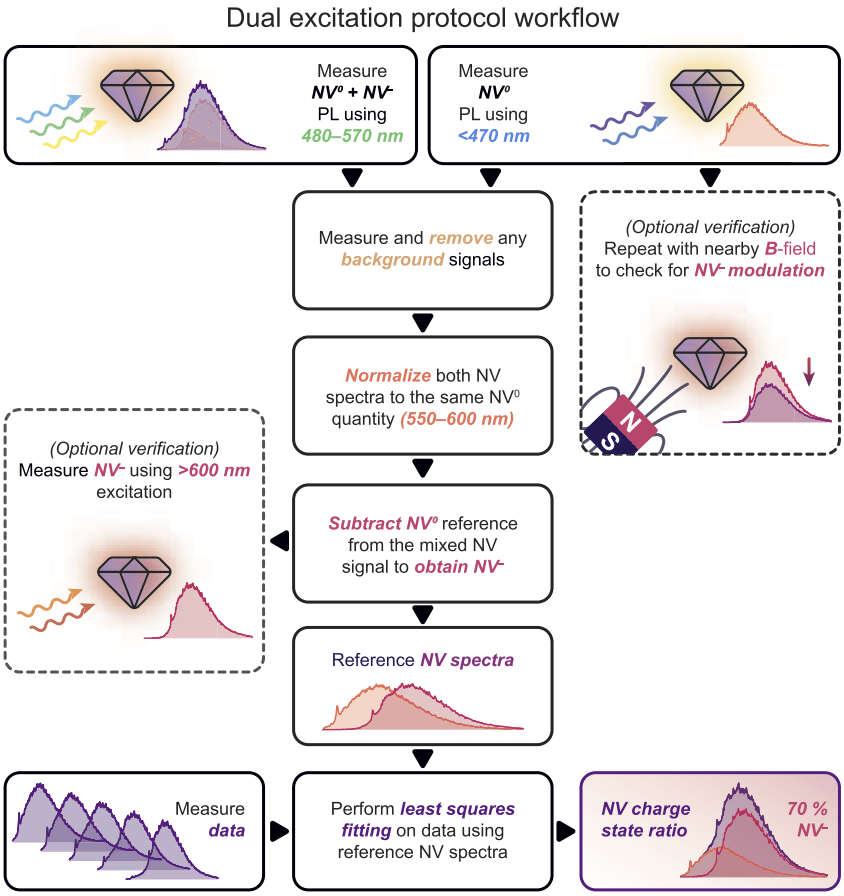

FIG. 4. Dual excitation protocol workflow. DEP requires two initial measurements taken with <470 nm and 480–570 nm to obtain reference NV^0 and mixed NV^0/NV^- spectra. Background signals must be removed from the two measurements before normalization between 550 and 600 nm. Once normalized, the difference between the signals can be calculated to obtain the NV^- reference spectrum. After both reference spectra are determined, they can be used to fit data to determine the relative contribution of each charge state.

from the diamond host or the surrounding media (e.g., water) in the case of FND suspensions.

Generally, the acquisition and subtraction of these background spectra are very effective, and we present a complex example of such background removal in the supplementary material, Fig. S9. Once all background signals are accounted for, the two spectra (NV^0 + NV^- and NV^0 only) are normalized between 550 and 600 nm to the same NV^0 contribution. Then, the NV^0 spectrum is subtracted from the spectrum containing both charge states to yield a pure NV^- reference spectrum. Finally, the two reference spectra can be fit to data of interest using a least squares fitting routine to determine the relative contribution of each NV charge state to the overall fluorescence signal.

C. Verification and refinement

Two optional steps can be introduced to verify the NV reference spectra. First, it is possible under certain conditions to observe NV^- PL using photon energies above 2.63 eV (below 470 nm), which would normally photoionize NV^- and create NV^0. Therefore, an additional step may be introduced to check for NV^- modulation under <470 nm excitation in an external magnetic field, which is known to affect the NV^- quantum yield[39,40] but not NV^0. Second, an excitation wavelength of >600 nm can be used to generate a pure NV^- spectrum. Generally, optical notch filters would be required to remove the excitation light signal from the PL spectrum, blocking part of the NV spectrum. Nevertheless, the resulting NV spectrum can be used to optimize the normalization window before the NV^0 reference is subtracted from the mixed NV^0/NV^- signal or used to remove any remaining NV^- in the NV^0 reference.

Here, we measure the NV fluorescence of a bulk diamond sample under both blue (430 nm) and red (630 nm) excitation wavelengths [Figs. 5(a) and 5(b), respectively] with and without the presence of an external magnetic field applied via a permanent magnet. Under blue excitation, Fig. 5(c) shows a 1.20% reduction in overall fluorescence when the magnet is introduced. Fitting the NV reference spectra using Eq. (1) allows us to approximate the change in fluorescence attributable to NV^-, which we find to be on the order of 0.18% [residuals in Fig. 5(e)]. We show that NV^- is reduced by 7.8% under the same applied $\vec{B}$-field, which we determine through red (630 nm) excitation and display in Fig. 5(d). Under this excitation condition, the change in fluorescence can be attributed solely to spin mixing induced by the magnetic field. Assuming that the total NV^- is also modulated to the same degree under 430 nm excitation, we can determine how much NV^- exists under 430 nm excitation via

$$\beta_0 = \frac{\Delta\beta}{C}, \tag{7}$$

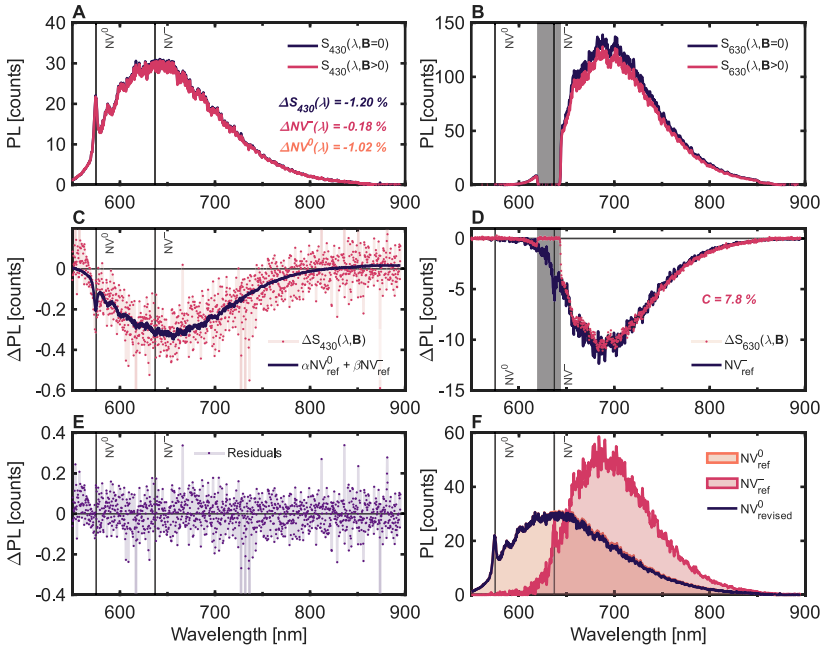

FIG. 5. NV fluorescence spectra measured using an excitation wavelength of 430 nm (a) and 630 nm (b) with and without the presence of an external $\vec{B}$-field, with the differences shown in (c) and (d), respectively. The change in fluorescence under 430 nm is fit with the NV reference spectra, with residuals shown in (e). (f) Original and revised NV reference spectra.

where β_0 is the NV^- scaling factor under no magnetic field, $\Delta\beta$ is the change in the NV^- scaling factor after the magnet is introduced, and C is the contrast observed under 630 nm [see Fig. 5(d)]. By approximating β_0, we can subtract any remaining NV^- from the NV^0 reference via

$$NV^0_{revised} = NV^0_{ref} - \beta_0 NV^-, \tag{8}$$

to obtain a revised NV^0 reference spectrum, which is ≈2% different from our original approximation as shown in Fig. 5(f). We note that this correction is still an approximation, as the fit used to determine $\Delta\beta$ uses an NV^0 reference, which may contain some small fraction of NV^- and, therefore, lead to a slight underestimate of $\Delta\beta$. Nevertheless, the change is relatively small, which increases our confidence that blue excitation is sufficient for NV charge state determination.

In our experiments and analysis, we do not explicitly consider two-photon processes, which may be present under pulsed and high-intensity continuous wave excitation and can affect NV charge state dynamics. The only measurement where this may affect the results of our protocol is the blue light excitation for the determination of the pure NV^0 spectrum. We employed a ps-pulsed laser in our experiments and found that residual NV^- emission in the NV^0 reference spectrum only leads to a small error, as discussed in the previous paragraph. We do not expect the pulsed excitation to play a major role here but encourage users of our protocol to check for residual NV^- PL in the NV^0 reference spectrum to obtain the most precise and reliable results.

IV. CONCLUSION

We investigated several approaches for calculating the NV^0/NV^- charge state ratio, particularly for diamond samples that do not exhibit pronounced zero-phonon lines (ZPLs), such as nanodiamonds. We tested ZPL fitting, two algorithmic approaches, namely fitting a skewed Gaussian model of the NV^0/NV^- spectral profiles and non-negative matrix factorization, and our dual excitation protocol (DEP), which employs blue (400–470 nm) and green (480–570 nm) excitation to derive a set of sample- and setup-specific pure NV^0/NV^- spectra to fit subsequent experiments. We evaluated each approach for a variety of different samples and optical systems, including bulk diamond and dispersed 100 nm nanodiamonds under a scanning confocal microscope, as well as 20 nm nanodiamonds in aqueous suspension. We demonstrate that DEP is capable of deriving quantitative NV charge state ratios that are consistent with our understanding of NV photophysics across common sample types and measurement setups.

SUPPLEMENTARY MATERIAL

Additional information, including optical setups, NV charge state ratio quantification protocol details, and additional data, can be found in the supplementary material.

ACKNOWLEDGMENTS

We acknowledge the support of the Australian Research Council (ARC) through a Discovery Project (Grant No. DP220102518) and the ARC Centre of Excellence in Quantum Biotechnology (Grant No. CE230100021). G.T. acknowledges support through an ARC Linkage Grant No. LP210300230 in collaboration with Diamond Defence Pty Ltd. D.J.M. acknowledges support through a University of Melbourne McKenzie Fellowship. N.D. acknowledges support through a Department of Defense NSDIRG Grant No. NS220100071. P.R. acknowledges support through an ARC DECRA Fellowship (Grant No. DE200100279) and an RMIT University Vice-Chancellor's Senior Research Fellowship. This study was

carried out in part at RMIT University's Microscopy and Microanalysis Facility, a linked laboratory of Microscopy Australia enabled by the National Collaborative Research Infrastructure Strategy (NCRIS).

AUTHOR DECLARATIONS

Conflict of Interest

The authors have no conflicts to disclose.

Author Contributions

G. Thalassinos: Conceptualization (lead); Formal analysis (lead); Investigation (lead); Methodology (lead); Software (lead); Visualization (lead); Writing – original draft (equal); Writing – review & editing (equal). **D. J. McCloskey**: Conceptualization (supporting); Writing – review & editing (equal). **A. Mameli**: Investigation (supporting); Writing – review & editing (supporting). **A. J. Healey**: Resources (equal); Writing – review & editing (equal). **C. Pattinson**: Writing – review & editing (equal). **D. Simpson**: Funding acquisition (equal); Supervision (equal); Writing – review & editing (supporting). **B. C. Gibson**: Funding acquisition (equal); Supervision (equal); Writing – review & editing (equal). **A. Stacey**: Conceptualization (supporting); Writing – review & editing (equal). **N. Dontschuk**: Conceptualization (supporting); Methodology (supporting); Writing – review & editing (equal). **P. Reineck**: Conceptualization (equal); Project administration (equal); Resources (equal); Supervision (equal); Writing – original draft (equal); Writing – review & editing (equal).

DATA AVAILABILITY

The data that support the findings of this study are available from the corresponding author upon reasonable request.

REFERENCES

[1] R. Schirhagl, K. Chang, M. Loretz, and C. L. Degen, "Nitrogen-vacancy centers in diamond: Nanoscale sensors for physics and biology," Annu. Rev. Phys. Chem. **65**, 83–105 (2014).
[2] S. Pezzagna and J. Meijer, "Quantum computer based on color centers in diamond," Appl. Phys. Rev. **8**, 011308 (2021).
[3] J. Wrachtrup and F. Jelezko, "Processing quantum information in diamond," J. Phys.: Condens. Matter **18**, S807 (2006).
[4] L. Rondin, J.-P. Tetienne, T. Hingant, J.-F. Roch, P. Maletinsky, and V. Jacques, "Magnetometry with nitrogen-vacancy defects in diamond," Rep. Prog. Phys. **77**, 056503 (2014).
[5] P. Neumann, I. Jakobi, F. Dolde, C. Burk, R. Reuter, G. Waldherr, J. Honert, T. Wolf, A. Brunner, J. H. Shim, D. Suter, H. Sumiya, J. Isoya, and J. Wrachtrup, "High-precision nanoscale temperature sensing using single defects in diamond," Nano Lett. **13**, 2738–2742 (2013).
[6] D. J. McCloskey, N. Dontschuk, A. Stacey, C. Pattinson, A. Nadarajah, L. T. Hall, L. C. L. Hollenberg, S. Prawer, and D. A. Simpson, "A diamond voltage imaging microscope," Nat. Photonics **16**, 730–736 (2022).
[7] F. Dolde, H. Fedder, M. W. Doherty, T. Nöbauer, F. Rempp, G. Balasubramanian, T. Wolf, F. Reinhard, L. C. L. Hollenberg, F. Jelezko, and J. Wrachtrup, "Electric-field sensing using single diamond spins," Nat. Phys. **7**, 459–463 (2011).
[8] Y. Doi, T. Fukui, H. Kato, T. Makino, S. Yamasaki, T. Tashima, H. Morishita, S. Miwa, F. Jelezko, Y. Suzuki, and N. Mizuochi, "Pure negatively charged state of the NV center in *n*-type diamond," Phys. Rev. B **93**, 081203 (2016).
[9] A. A. Wood, A. Lozovoi, R. M. Goldblatt, C. A. Meriles, and A. M. Martin, "Wavelength dependence of nitrogen vacancy center charge cycling," Phys. Rev. B **109**, 134106 (2024).
[10] J. F. Barry, J. M. Schloss, E. Bauch, M. J. Turner, C. A. Hart, L. M. Pham, and R. L. Walsworth, "Sensitivity optimization for NV-diamond magnetometry," Rev. Mod. Phys. **92**, 015004 (2020).
[11] L. Rondin, G. Dantelle, A. Slablab, F. Grosshans, F. Treussart, P. Bergonzo, S. Perruchas, T. Gacoin, M. Chaigneau, H.-C. Chang, V. Jacques, and J.-F. Roch, "Surface-induced charge state conversion of nitrogen-vacancy defects in nanodiamonds," Phys. Rev. B **82**, 115449 (2010).
[12] N. B. Manson, M. Hedges, M. S. J. Barson, R. Ahlefeldt, M. W. Doherty, H. Abe, T. Ohshima, and M. J. Sellars, "NV^-–N^+ pair centre in 1b diamond," New J. Phys. **20**, 113037 (2018).
[13] N. Aslam, G. Waldherr, P. Neumann, F. Jelezko, and J. Wrachtrup, "Photo-induced ionization dynamics of the nitrogen vacancy defect in diamond investigated by single-shot charge state detection," New J. Phys. **15**, 013064 (2013).
[14] V. M. Acosta, E. Bauch, M. P. Ledbetter, C. Santori, K.-M. C. Fu, P. E. Barclay, R. G. Beausoleil, H. Linget, J. F. Roch, F. Treussart, S. Chemerisov, W. Gawlik, and D. Budker, "Diamonds with a high density of nitrogen-vacancy centers for magnetometry applications," Phys. Rev. B **80**, 115202 (2009).
[15] S. T. Alsid, J. F. Barry, L. M. Pham, J. M. Schloss, M. F. O'Keeffe, P. Cappellaro, and D. A. Braje, "Photoluminescence decomposition analysis: A technique to characterize N-*V* creation in diamond," Phys. Rev. Appl. **12**, 044003 (2019).
[16] K.-M. C. Fu, C. Santori, P. E. Barclay, and R. G. Beausoleil, "Conversion of neutral nitrogen-vacancy centers to negatively charged nitrogen-vacancy centers through selective oxidation," Appl. Phys. Lett. **96**, 121907 (2010).
[17] C. Shinei, M. Miyakawa, S. Ishii, S. Saiki, S. Onoda, T. Taniguchi, T. Ohshima, and T. Teraji, "Equilibrium charge state of NV centers in diamond," Appl. Phys. Lett. **119**, 254001 (2021).
[18] N. B. Manson and J. P. Harrison, "Photo-ionization of the nitrogen-vacancy center in diamond," Diamond Relat. Mater. **14**, 1705–1710 (2005).
[19] S. Eldemrdash, G. Thalassinos, A. Alzahrani, Q. Sun, E. Walsh, E. Grant, H. Abe, T. L. Greaves, T. Ohshima, P. Cigler, P. Matějíček, D. A. Simpson, A. D. Greentree, G. Bryant, B. C. Gibson, and P. Reineck, "Fluorescent HPHT nanodiamonds have disk- and rod-like shapes," Carbon **206**, 268–276 (2023).
[20] C. Bradac, T. Gaebel, N. Naidoo, M. J. Sellars, J. Twamley, L. J. Brown, A. S. Barnard, T. Plakhotnik, A. V. Zvyagin, and J. R. Rabeau, "Observation and control of blinking nitrogen-vacancy centres in discrete nanodiamonds," Nat. Nanotechnol. **5**, 345 (2010).
[21] O. Shenderova, N. Nunn, T. Oeckinghaus, M. Torelli, G. McGuire, K. Smith, E. Danilov, R. Reuter, J. Wrachtrup, A. Shames, D. Filonova, and A. Kinev, "Commercial quantities of ultrasmall fluorescent nanodiamonds containing color centers," Proc. SPIE **10118**, 1011803 (2017).
[22] K. Groot-Berning, N. Raatz, I. Dobrinets, M. Lesik, P. Spinicelli, A. Tallaire, J. Achard, V. Jacques, J.-F. Roch, A. M. Zaitsev, J. Meijer, and S. Pezzagna, "Passive charge state control of nitrogen-vacancy centres in diamond using phosphorous and boron doping," Phys. Status Solidi A **211**, 2268–2273 (2014).
[23] S. Dhomkar, H. Jayakumar, P. R. Zangara, and C. A. Meriles, "Charge dynamics in near-surface, variable-density ensembles of nitrogen-vacancy centers in diamond," Nano Lett. **18**, 4046–4052 (2018).
[24] M. W. Doherty, V. M. Acosta, A. Jarmola, M. S. J. Barson, N. B. Manson, D. Budker, and L. C. L. Hollenberg, "Temperature shifts of the resonances of the NV^- center in diamond," Phys. Rev. B **90**, 041201 (2014).
[25] D. Aude Craik, P. Kehayias, A. Greenspon, X. Zhang, M. Turner, J. Schloss, E. Bauch, C. Hart, E. Hu, and R. Walsworth, "Microwave-assisted spectroscopy technique for studying charge state in nitrogen-vacancy ensembles in diamond," Phys. Rev. Appl. **14**, 014009 (2020).
[26] H.-Q. Zhao, M. Fujiwara, and S. Takeuchi, "Suppression of fluorescence phonon sideband from nitrogen vacancy centers in diamond nanocrystals by substrate effect," Opt. Express **20**, 15628–15635 (2012).

[27]P. Reineck, L. F. Trindade, J. Havlik, J. Stursa, A. Heffernan, A. Elbourne, A. Orth, M. Capelli, P. Cigler, D. A. Simpson, and B. C. Gibson, "Not all fluorescent nanodiamonds are created equal: A comparative study," Part. Part. Syst. Charact. **36**, 1900009 (2019).
[28]E. R. Wilson, L. M. Parker, A. Orth, N. Nunn, M. Torelli, O. Shenderova, B. C. Gibson, and P. Reineck, "The effect of particle size on nanodiamond fluorescence and colloidal properties in biological media," Nanotechnology **30**, 385704 (2019).
[29]D. J. McCloskey, N. Dontschuk, D. A. Broadway, A. Nadarajah, A. Stacey, J.-P. Tetienne, L. C. L. Hollenberg, S. Prawer, and D. A. Simpson, "Enhanced widefield quantum sensing with nitrogen-vacancy ensembles using diamond nanopillar arrays," ACS Appl. Mater. Interfaces **12**, 13421–13427 (2020).
[30]S. A. Savinov, V. V. Sychev, and D. Bi, "Diamond nitrogen-vacancy center charge state ratio determination at a given sample point," J. Lumin. **248**, 118981 (2022).
[31]A. Bhaumik, R. Sachan, and J. Narayan, "Tunable charge states of nitrogen-vacancy centers in diamond for ultrafast quantum devices," Carbon **142**, 662–672 (2019).
[32]F. Treussart, V. Jacques, E. Wu, T. Gacoin, P. Grangier, and J.-F. Roch, "Photoluminescence of single colour defects in 50 nm diamond nanocrystals," Physica B **376**, 926–929 (2006).
[33]S. Karaveli, O. Gaathon, A. Wolcott, R. Sakakibara, O. A. Shemesh, D. S. Peterka, E. S. Boyden, J. S. Owen, R. Yuste, and D. Englund, "Modulation of nitrogen vacancy charge state and fluorescence in nanodiamonds using electrochemical potential," Proc. Natl. Acad. Sci. U. S. A. **113**, 3938–3943 (2016).
[34]L. Razinkovas, M. Maciaszek, F. Reinhard, M. W. Doherty, and A. Alkauskas, "Photoionization of negatively charged NV centers in diamond: Theory and *ab initio* calculations," Phys. Rev. B **104**, 235301 (2021).
[35]Á. Gali, "Recent advances in the *ab initio* theory of solid-state defect qubits," Nanophotonics **12**, 359–397 (2023).
[36]E. Bourgeois, E. Londero, K. Buczak, J. Hruby, M. Gulka, Y. Balasubramaniam, G. Wachter, J. Stursa, K. Dobes, F. Aumayr, M. Trupke, A. Gali, and M. Nesladek, "Enhanced photoelectric detection of NV magnetic resonances in diamond under dual-beam excitation," Phys. Rev. B **95**, 041402 (2017).
[37]T.-I. Yang, Y.-W. Huang, P. Bista, C.-F. Ding, J. Chen, C.-T. Chiang, and H.-C. Chang, "Photoluminescence of nitrogen-vacancy centers by ultraviolet one- and two-photon excitation of fluorescent nanodiamonds," J. Phys. Chem. Lett. **13**, 11280–11287 (2022).
[38]K. Beha, A. Batalov, N. B. Manson, R. Bratschitsch, and A. Leitenstorfer, "Optimum photoluminescence excitation and recharging cycle of single nitrogen-vacancy centers in ultrapure diamond," Phys. Rev. Lett. **109**, 097404 (2012).
[39]M. Capelli, P. Reineck, D. W. M. Lau, A. Orth, J. Jeske, M. W. Doherty, T. Ohshima, A. D. Greentree, and B. C. Gibson, "Magnetic field-induced enhancement of the nitrogen-vacancy fluorescence quantum yield," Nanoscale **9**, 9299–9304 (2017).
[40]J.-P. Tetienne, L. Rondin, P. Spinicelli, M. Chipaux, T. Debuisschert, J.-F. Roch, and V. Jacques, "Magnetic-field-dependent photodynamics of single NV defects in diamond: An application to qualitative all-optical magnetic imaging," New J. Phys. **14**, 103033 (2012).